



Inactivation of the phenylpyruvate tautomerase activity of macrophage migration inhibitory factor by 2-oxo-4-phenyl-3-butynoate [☆]

Pavel A. Golubkov ^a, William H. Johnson Jr. ^b,
Robert M. Czerwinski ^b, Maria D. Person ^c, Susan C. Wang ^b,
Christian P. Whitman ^{b,*}, Marvin L. Hackert ^{a,*}

^a Department of Chemistry and Biochemistry, University of Texas at Austin, Austin, TX 78712, USA

^b Division of Medicinal Chemistry, College of Pharmacy, University of Texas at Austin, Austin, TX 78712, USA

^c Division of Pharmacology and Toxicology, College of Pharmacy, University of Texas at Austin, Austin, TX 78712, USA

Received 23 March 2006

Available online 14 June 2006

Abstract

Macrophage migration inhibitory factor (MIF) is an important immunoregulatory protein that has been implicated in several inflammatory diseases. MIF also has a phenylpyruvate tautomerase (PPT) activity, the role of which remains elusive in these biological activities. The acetylene compound, 2-oxo-4-phenyl-3-butynoate (2-OPB), has been synthesized and tested as a potential irreversible inhibitor of its enzymatic activity. Incubation of the compound with MIF results in the rapid and irreversible loss of the PPT activity. Mass spectral analysis established that the amino-terminal proline, previously implicated as a catalytic base in the PPT-catalyzed reaction, is the site of covalent modification. Inactivation of the PPT activity likely occurs by a Michael addition of Pro-1 to C-4 of the inhibitor. Attempts to crystallize the inactivated complex to confirm the structure of the adduct on the covalently modified Pro-1 by X-ray crystallography were not successful. Nor was it possible to unambiguously interpret electron density observed in the active sites of the native crystals soaked with the inhibitor. This may be due to crystal packing in that the side chain of Glu-16 from an

[☆] This research was supported by the National Institutes of Health Grant GM-65324 (C.P.W. and M.L.H.) and the Robert A. Welch Foundation (F-1219 to M.L.H.). SCW is a Fellow of the American Foundation for Pharmaceutical Education.

* Corresponding authors. Fax: +1 512 471 6135 (M.L. Hackert), +1 512 232 2606 (C.P. Whitman).

E-mail addresses: whitman@mail.utexas.edu (C.P. Whitman), m.hackert@mail.utexas.edu (M.L. Hackert).

adjacent trimer occupies one active site. However, this crystal contact may be partially responsible for the high-resolution quality of these MIF crystals. Nonetheless, because MIF is a member of the tautomerase superfamily, a group of structurally homologous proteins that share a β - α - β structural motif and a catalytic Pro-1, 2-OPB may find general use as a probe of tautomerase superfamily members that function as PPTs.

© 2006 Elsevier Inc. All rights reserved.

Keywords: Enzyme; Inactivation; MIF; Acetylene compound

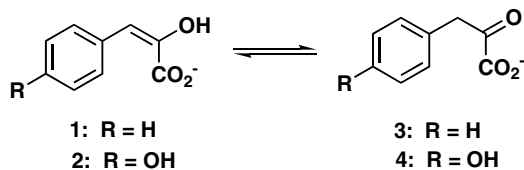
1. Introduction

Macrophage migration inhibitory factor (MIF)¹ was first identified in the 1960s as a protein involved in delayed-type hypersensitivity responses [1–3]. Since its initial discovery, MIF has been implicated in several inflammatory and autoimmune diseases, including arthritis [4–7], glomerulonephritis [8], and Gram-positive and Gram-negative sepsis [9,10]. The pro-inflammatory properties of MIF are coupled with an ability to counter the effect of corticosteroids [9,11]. Thus, MIF inhibitors are of considerable interest as potential anti-inflammatory agents. MIF also exhibits a phenylpyruvate tautomerase (PPT) activity, catalyzing the ketonization of the enol isomers of phenylpyruvate (**1**, Scheme 1) [12] and *p*-hydroxyphenylpyruvate (**2**) to the respective keto isomers (**3** and **4**) [13]. Despite intense study, cellular receptors for MIF and the relevance of the enzymatic activity to the biological activities remain unknown.

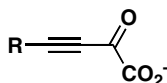
Three-dimensional X-ray crystallographic studies of human and murine MIF demonstrate that MIF exists as a homotrimer and is structurally related to the bacterial 4-oxalocrotonate tautomerase (4-OT) and 5-carboxymethyl-2-hydroxymuconate isomerase (CHMI) [14,15] despite low (<20%) sequence identity with these enzymes. Thus, MIF is a member of the tautomerase superfamily, a group of structurally homologous proteins characterized by a common β - α - β fold and a catalytic amino-terminal proline [16]. Pro-1 has been implicated as a critical residue in the PPT activity [13,17].

The acetylene compounds, 2-oxo-3-pentynoate (2-OP, **5**, Scheme 2) and 2-oxo-3-butynoate (2-OB, **6**), are active-site-directed, irreversible inhibitors of 4-OT [18,19]. Both compounds form a covalent bond with the amino-terminal proline, which functions as the general base in the 4-OT-catalyzed reaction. More significantly, crystallographic analysis of 4-OT inactivated by 2-OP provided much of the information about the positioning of active site residues and resulted in a proposed mechanism for the 4-OT-catalyzed reaction. The structural and functional similarities between 4-OT and MIF, which also uses Pro-1 as the catalytic base in the PPT-catalyzed reaction, suggested that the acetylene analogue of

¹ *Abbreviations used:* APS, advanced photon source; ARP, automated refinement procedure; CHMI, 5-carboxymethyl-2-hydroxymuconate isomerase; *cis*-CaaD, *cis*-3-chloroacrylic acid dehalogenase; ESI-MS, electrospray ionization mass spectrometry; F_o and F_c , observed and calculated structure factors, respectively; HPLC, high pressure liquid chromatography; Kn, kanamycin; MIF, macrophage migration inhibitory factor; MSAD, malonate semialdehyde decarboxylase; MALDI-PSD, matrix assisted laser desorption–ionization post-source decay; MALDI-TOF, matrix assisted laser desorption–ionization time-of-flight; NCS, non-crystallographic symmetry; 4-OT, 4-oxalocrotonate tautomerase; 2-OPB, 2-oxo-4-phenyl-3-butynoate; 2-OP, 2-oxo-3-pentynoate; 2-OB, 2-oxo-3-butynoate; PPT, phenylpyruvate tautomerase; rmsd, root-mean-square deviation; SDS–PAGE, sodium dodecyl sulfate–polyacrylamide gel electrophoresis.



Scheme 1.



- 5: R = CH₃**
6: R = H
7: R = Phenyl

Scheme 2.

5, 2-oxo-4-phenyl-3-butynoate (2-OPB, **7**, Scheme 2) might be an irreversible inhibitor of MIF and a comparable diagnostic probe for exploring the enzymatic reactions as well as the biological activities. Hence, 2-OPB was synthesized and evaluated as a potential irreversible inhibitor of MIF. In addition, a structure of MIF crystals soaked with **7** has been determined to 1.45 Å resolution. The results are reported herein.

2. Materials and methods

Materials. All reagents, buffers, and solvents were obtained from Sigma–Aldrich Chemical Co. (St Louis, MO) with the following exceptions. The syntheses of *tert*-butyl glyoxylate (**10**) and (*E*)-2-fluoro-*p*-hydroxycinnamate (**13**) have been described [18,20]. Recombinant murine MIF was purified as described previously [15]. Isopropyl-β-D-thiogalactoside (IPTG) and thin-walled PCR tubes were obtained from Ambion, Inc. (Austin, TX). Pre-packed PD-10 Sephadex G-25 columns were purchased from Biosciences AB (Uppsala, Sweden). Bacterial culture media, PCR reagents, molecular biology kits and reagents, oligonucleotide primers, and the bacterial strains used for the construction of the expression vector were obtained from the sources listed elsewhere [21].

Methods. Techniques for restriction enzyme digestions, ligation, transformation, and other standard molecular biology manipulations were based on methods described elsewhere [22]. DNA sequencing was done at the University of Texas (Austin) Sequencing Facility. Kinetic data and UV absorbance readings were obtained on a Hewlett–Packard 8452A Diode Array spectrophotometer. The kinetic data were fitted by nonlinear regression data analysis using the Grafit program (Erithacus Software Ltd., Staines, UK) obtained from Sigma–Aldrich Chemical Co. HPLC was performed on a Waters 501/510 system using a TSKgel DEAE-5PW (150 × 21.5 mm) column (Tosoh Bioscience, Montgomeryville, PA). Protein was analyzed by tricine sodium dodecyl sulfate-polyacrylamide gel electrophoresis (SDS–PAGE) under denaturing conditions on 16% gels on a vertical gel electrophoresis apparatus obtained from Bio-Rad (Hercules, CA) [23]. Protein concentrations were determined using the method of Waddell [24]. NMR spectra were obtained

on a Varian UNITY-plus 300 MHz spectrometer. Chemical shifts were referenced as noted below. Mass spectral data were obtained on an LCQ electrospray ion-trap mass spectrometer (ThermoFinnigan, San Jose, CA) or a delayed extraction Voyager-DE PRO matrix-assisted laser desorption/ionization time-of-flight (MALDI-TOF) instrument (PerSeptive Biosystems, Framingham, MA), as indicated below. Both instruments are housed in the Analytical Instrumentation Facility Core in the College of Pharmacy at the University of Texas at Austin.

2.1. Chemical syntheses

Preparation of tert-butyl 2-hydroxy-4-phenyl-3-butynoate (11). Methylmagnesium bromide (1.05 equiv.) in ether was added dropwise over a 20 min period to a stirring solution of phenylacetylene (**8**, 2.4 g, 23.1 mmol) dissolved in 15 mL of anhydrous THF at room temperature and under argon. The reaction mixture was warmed and gently refluxed. After stirring overnight, the reaction mixture was cooled to -78°C . Subsequently, *tert*-butyl glyoxylate (**10**, 3.0 g, 23.1 mmol) dissolved in 7 mL THF was added rapidly. The reaction mixture was allowed to warm to room temperature over a 2 h period and added to a 10% NaH_2PO_4 solution (200 mL). The resulting mixture was extracted with a mixture of hexanes and ethyl acetate (2:1, 3×200 mL). The organic layers were pooled, dried over anhydrous Na_2SO_4 , and concentrated to dryness to give crude product, **11**, as a yellow liquid (~ 6.1 g). The crude product was used in the next step without further purification.

Preparation of tert-butyl 2-oxo-4-phenyl-3-butynoate (12). To a solution of **11** in 50 mL of anhydrous CH_2Cl_2 was added activated MnO_2 (25 g) in small portions. The resulting reaction mixture was stirred overnight at room temperature and then stirred for another night at 6°C . Subsequently, the reaction mixture was filtered through a silica gel plug column in order to remove the MnO_2 and the filtrate was concentrated under reduced pressure. The residue was subjected to flash chromatography (8:1 hexanes, ethyl acetate). The UV active fractions were collected and concentrated to give a yellow solid (3.0 g). ^1H NMR (CDCl_3 , 300 MHz): δ 1.61 (9H, s), 7.42 (2H, t, *m*-H), 7.52 (1H, triplet of triplets, *p*-H), 7.66 (2H, dd, *o*-H). ^{13}C NMR (CDCl_3 , 75.5 MHz): δ 28.0 (CH_3 of *t*-butyl), 87.0 (C-4), 85.2 (C of *t*-butyl), 97.6 (C-3), 119.5 (C_α), 129.0 (C_γ), 131.9 (C_δ), 133.9 (C_β), 158.4 (C-1), 171.1 (C-2). HRMS m/z calculated for $\text{C}_{10}\text{H}_7\text{O}_3$ (MH^+) 231.1021, found 231.1021.

Preparation of 2-oxo-4-phenyl-3-butynoate (7). The *tert*-butyl group was removed by a literature procedure [18]. Accordingly, **12** (0.33 g, 1.4 mmol) was treated with trifluoroacetic acid as described [18] to yield **7** (0.25 g) in 100% yield. ^1H NMR (CDCl_3 , 300 MHz): δ 7.47 (2H, t, *m*-H), 7.55 (1H, triplet of triplets, *p*-H), 7.69 (2H, dd, *o*-H). ^{13}C NMR (CDCl_3 , 75.5 MHz): δ 86.8 (C-4), 101.4 (C-3), 119.0 (C_α), 129.1 (C_γ), 132.5 (C_δ), 134.3 (C_β), 159.4 (C-1), 170.6 (C-2). HRMS m/z calculated for $\text{C}_{10}\text{H}_7\text{O}_3$ (MH^+) 175.0395, found 175.0400.

2.2. Site-directed mutagenesis and enzymology methods

Construction of the E16A MIF-mutant. The E16A-MIF mutant was constructed by overlap extension PCR as described elsewhere [25]. The external primers for the construction of the mutant were oligonucleotides 5'-GCG GAT AAC AAT TCC CCT CT-3' (primer A) and 5'-CTC AGC TTC CTT TCG GGC TT-3' (primer D). Primer A corresponds to a region 36 bases upstream of the *Nde*I restriction site in the pET-24a(+)

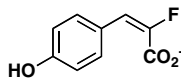
plasmid, while primer D corresponds to the complementary sequence of a region 20 bases downstream of the His-tag region in the pET-24a(+) plasmid. The internal primers were 5'-CAG AAA CCC CGC TGG CAC G-3' (primer B) and 5'-C GTG CCA GCG GGG TTT CTG-3' (primer C). In primers B and C, the mutation is underlined. The remaining bases correspond to the nucleotide coding sequence (primer C) or the complementary sequence (primer B) of the gene.

For the construction of the AB and CD fragments, each reaction mixture contained 1 μL of a 20 μM solution of primers A and B or primers C and D, 5 μL 10 \times high fidelity buffer, 1 μL 10 mM dNTPs, 2 μL 50 mM MgSO_4 , 5 μL of a 1:500 dilution of pET-11b MIF, 0.4 μL of platinum Taq high fidelity, and a sufficient quantity of sterile water to make a final volume of 50 μL . The PCR protocol consisted of an initial 45-s incubation period at 94 $^\circ\text{C}$, followed by 35 cycles of the PCR where each cycle contained a denaturation step at 94 $^\circ\text{C}$ for 30 s, an annealing step at 50 $^\circ\text{C}$ for 45 s, and an elongation step at 68 $^\circ\text{C}$ for 2 min, and a final 10-min incubation period at 68 $^\circ\text{C}$. The PCR products were purified by gel electrophoresis followed by use of the Ultrafree-DA centrifugal units. The AD fragment was constructed similarly except that the AB and CD fragments (2 μL of each) were used as template. The AD fragment was electrophoresed, excised, and purified using the Ultrafree-DA centrifugal unit. Restriction digests of the AD fragment and the pET-24a(+) vector were performed with the *NdeI* and *BamHI* enzymes as described elsewhere [22]. The digested fragments were purified by electrophoresis followed by use of the Ultrafree-DA units and ligated using the Quick Ligation Kit (New England Biolabs). The DNA was purified by ethanol precipitation and used to transform *Escherichia coli* strain BL21-Gold(DE3)pLysS by electroporation according to the manufacturer's instructions. Transformed cells were plated onto LB/Kn (50 $\mu\text{g}/\text{mL}$) and incubated overnight at 37 $^\circ\text{C}$. A randomly selected colony, designated pET-24a-E16A-MIF2, had the correct sequence for the desired mutation with no other changes.

Expression and purification of the E16A-MIF mutant. The E16A-MIF mutant was grown and purified under the conditions described elsewhere [15] except the Sephadex G-75 column was equilibrated and eluted using 20 mM NaH_2PO_4 buffer, pH 7.3. Under these conditions, 3 L of culture yields ~ 5 g of cells and ~ 95 mg of protein purified to near homogeneity ($\sim 95\%$ as assessed by SDS-PAGE).

Kinetics of irreversible inhibition of MIF by 2-OPB (7). The inhibition of the enzymatic activity of MIF by **7** was carried out at 0 $^\circ\text{C}$ as follows. Incubation mixtures (total volume = 1.0 mL) containing different concentrations of **7** (0–100 μM from stock solutions) and MIF (48 μM based on subunit molecular mass) in 50 mM NaH_2PO_4 buffer (pH 6.0) were made up in 1.5 mL Eppendorf micro test tubes. Aliquots were removed at various time intervals (0, 5, 10, 15, 30, 60, and 120 s) and the residual PPT activity was assayed following the disappearance of the enol isomer of phenylpyruvic acid (**1**, 2.5 mM) at 288 nm as described [15].

Protection of the PPT activity from inactivation by 13. The competitive inhibitor, (*E*)-2-fluoro-*p*-hydroxycinnamate (**13**) [15,20], was pre-incubated with MIF in order to protect the PPT activity from inactivation by **7**. Accordingly, various concentrations of **13** (0–250 μM) were incubated with MIF (50 μM based on subunit molecular mass) in 50 mM NaH_2PO_4 buffer (1 mL, pH 6.8) for 5 min. Subsequently, **7** (60 μM) was added to the mixture. Aliquots (5 μL) were removed at various time intervals (0, 5, 10, 15, 30, 60, and 120 s) and added to the boric acid assay mixture (1 mL) in order to stop the reaction. The components of this mixture and the assay are described elsewhere [20].



13

Irreversibility of the inactivation. MIF (0.4 μmol based on subunit molecular mass) and **7** (4 μmol) were incubated in 50 mM NaH_2PO_4 buffer (final volume 10 mL, pH 6.8) for 5 min at 4 °C. In a separate control reaction, the same quantity of MIF was incubated without **7** under otherwise identical conditions. Both samples were dialyzed against 50 mM NaH_2PO_4 buffer (pH 6.8) for 68 h. Aliquots were removed and assayed for residual activity using the enol isomer of phenylpyruvic acid (**1**) as described [15].

Mass spectral analysis of modified MIF. To a quantity of MIF (2 mg, 0.16 μmol based on subunit molecular mass) in 1 mL of 20 mM NaH_2PO_4 (pH 7.3) on ice were added 3–5 μL portions of **7** (5.7 mM solution, 0.03 μmol per aliquot) at 5 min intervals. There was no activity (as determined following the disappearance of **1**) after the addition of the third aliquot. The incubation mixtures containing the inactivated MIF or the control sample (incubated without **7**) were loaded onto separate PD-10 Sephadex G-25 gel filtration columns, which had previously been equilibrated with 10 mM NH_4HCO_3 buffer (pH 8.0) as described [26]. The mixtures were processed and the resulting proteins analyzed by electrospray ionization mass spectrometry (ESI-MS) as described (26). The same samples were used in the peptide mapping experiments described below.

Peptide mapping. A sample of MIF or MIF modified by **7** (after elution from the gel filtration column) was treated with sequencing grade trypsin as described [26]. Subsequently, the trypsin treated samples were analyzed by matrix assisted laser desorption–ionization time-of-flight (MALDI-TOF) mass spectrometry [26]. Selected ions in the samples were subjected to MALDI-post-source decay (PSD) analysis using the protocol described elsewhere [26,27].

2.3. Crystallography methods

Crystallization. Crystals of murine MIF were grown by vapor diffusion from 24 to 30% PEG 8000 in 50 mM NaH_2PO_4 buffer at pH 7.0, 5 μL (20 mg/mL) MIF, and 5 μL of well solution per droplet. All of the crystals from one hanging drop (~ 0.1 mg protein) were transferred into 200 μL of 30% PEG 8000, 50 mM NaH_2PO_4 buffer at pH 7.0, and soaked in a 2-fold excess (~ 0.1 mM) of **7** for 40 h.

Data collection. Crystals were cryoprotected with 30% PEG 8000 and flash-cooled in liquid nitrogen. The crystal used for data collection was maintained at 100 K in a gaseous nitrogen stream provided by an Oxford Cryo-Jet system. X-ray diffraction intensities were measured to 1.45 Å resolution with a Quantum 4 CCD detector using synchrotron radiation at the advanced photon source (APS) beamline 14-BMD (BioCARS). The energy used was 12.660 keV (0.97935 Å). The crystal-to-detector distance was 120 mm. A total of 80 frames were collected with a 1° interval at an exposure of 45 s per frame. The intensity data were collected from a single crystal, scaled, and merged at the APS using the HKL-2000 program package [28]. The data collection statistics are summarized in Table 1.

Structure determination and refinement. The space group is $P6_3$ with $a = 94.71$ and $c = 87.67$ Å. Assuming one trimer per asymmetric unit, the Matthews' coefficient [29] is 3.3 Å³/Da and the implied solvent content is 63% [30]. The model used for molecular

Table 1

Data collection and refinement statistics

<i>Data-collection statistics</i>	
Space group	P6 ₃
Unit-cell parameters	
<i>a</i> = <i>b</i> (Å)	94.71
<i>c</i> (Å)	87.67
Temperature (K)	100
Wavelength (Å)	0.9794
Resolution range (Å)	50.0–1.45 (1.49–1.45)
<i>R</i> _{merge} (%)	4.7
Completeness (%)	97.4 (96.8)
$\langle I/\sigma(I) \rangle$	10.3
No. measured reflections	676,784
No. unique reflections	78,898
No. >3 σ	76,875
Mosaicity (°)	0.376
<i>Refinement statistics</i>	
No. working reflections	73,003 (5323)
No. test set reflections	3872 (278)
<i>R</i> _{work}	0.14 (0.22) ^a
<i>R</i> _{free}	0.18 (0.30)
Protein atoms	2606
Water molecules	465
<i>Geometry statistics</i>	
rmsd, bond lengths (Å)	0.05
rmsd, bond angles (°)	3.57
Average B value for all atoms (Å ²)	22.1
Average B value for main chain	17.2
Average B value for side chain and waters	26.0
Average rms B for 342 main-chain residues	1.11
Average rms B for 288 side-chain residues	3.12
Overall correlation coefficient	0.975
Overall figure of merit	0.897

^a X-ray diffraction data were collected to a low-resolution limit of 50.0 Å, but the refinement was carried out with the data between 23.8 and 1.45 Å resolution.

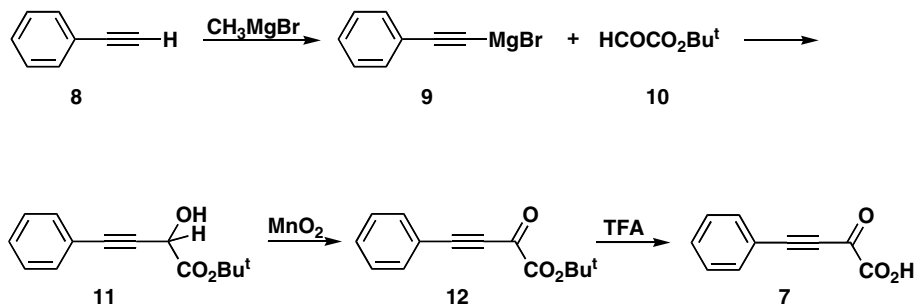
replacement was that of the Y95F mutant of MIF (PDB entry 1MFF) [31]. The program suite CCP4 (Collaborative Computational Project, Number 4) [32] using the graphic user interface ccp4i [33] for MOLREP and AMORE [34] was used for obtaining rotational and translational parameters. The best molecular replacement solution had an *R* value of 0.354 and a correlation coefficient of 0.675. REFMAC5 was used for maximum-likelihood refinement [35]. The initial round of refinement, conducted with non-crystallographic symmetry (NCS) constraints, geometric restraints, and translation, libration, screw (TLS) groups [36], lowered *R* to 0.27 and *R*_{free} to 0.29. The graphics program O [37] was used to adjust the model to fit the resulting electron density map generated by FFT [38]. The high quality of the electron density map was immediately apparent as the map clearly showed the tyrosine at position 95 when using phases derived from the Y95F mutant model. In later stages of refinement NCS constraints were removed and the B-factors were refined anisotropically. Solvent molecules were added by a combination of automatic

identification by a routine in automated refinement procedure ARP/wARP [39] and manual insertions in the program O using O macro written by Gerard Kleywegt. The refined structure contains 2606 protein atoms and 465 water molecules with R and R_{free} of 0.14 and 0.18, respectively, with excellent geometry as evidenced by the fact that 100% of all non-glycine, non-proline residues fall within the most-favored (92.4%) or additionally allowed (7.6%) regions of the Ramachandran plot. The refinement statistics are summarized in Table 1.

3. Results

Synthesis of 2-oxo-4-phenyl-3-butynoate (7). The synthesis of **7** is outlined in Scheme 3 and is analogous to the procedure used for the synthesis of 2-OP [19]. Accordingly, the magnesium bromide salt of phenylacetylene was generated in situ from the commercially available compounds, methylmagnesium bromide and phenylacetylene (**8**). Subsequent condensation of **9** with the *tert*-butyl ester of glyoxylate (**10**) produced **11**. Oxidation of **11** by activated MnO_2 yielded **12** as the major product after flash chromatography. The *tert*-butyl group was removed by anhydrous trifluoroacetic acid to result in the formation of **7** as the free acid. The ^1H and ^{13}C NMR spectra and mass spectral data are consistent with the structure of **7**.

Construction and characterization of the E16A mutant of MIF. The E16A mutant of MIF was constructed by overlap extension PCR [25], expressed in *E. coli* strain BL21(DE3)pLysS, and purified to >95% (as determined by SDS–PAGE) using a modification of a previously described procedure [15]. The DNA sequence of the mutant was confirmed by DNA sequencing. The steady-state kinetic parameters for the PPT activity of the E16A mutant were measured using **1** and **2** as substrates, and compared to the parameters for the PPT activity of wild-type MIF [31]. The PPT activity of E16A-MIF converts **1** to **3** (Scheme 1) with a $K_m = 160 \pm 40 \mu\text{M}$, a $k_{\text{cat}} = 200 \pm 30 \text{ s}^{-1}$, and a $k_{\text{cat}}/K_m = 1.25 \times 10^6 \text{ M}^{-1} \text{ s}^{-1}$. These values are comparable to those measured for the PPT activity of wild-type MIF ($K_m = 150 \pm 40 \mu\text{M}$, $k_{\text{cat}} = 320 \pm 80 \text{ s}^{-1}$, and $k_{\text{cat}}/K_m = 2.1 \times 10^6 \text{ M}^{-1} \text{ s}^{-1}$) [31]. The PPT activity of E16A-MIF converts **2** to **4** (Scheme 1) with a $K_m = 100 \pm 10 \mu\text{M}$, a $k_{\text{cat}} = 60 \pm 5 \text{ s}^{-1}$, and a $k_{\text{cat}}/K_m = 6.0 \times 10^5 \text{ M}^{-1} \text{ s}^{-1}$. These values are also comparable to those measured for the PPT activity of wild type MIF ($K_m = 200 \pm 70 \mu\text{M}$, $k_{\text{cat}} = 140 \pm 20 \text{ s}^{-1}$, and $k_{\text{cat}}/K_m = 7.0 \times 10^5 \text{ M}^{-1} \text{ s}^{-1}$) [31]. Hence, for both substrates, the kinetic parameters for the PPT activity of E16A-MIF



are not significantly different from those measured for the wild type. These results are consistent with the observation that Glu-16 is not in the active site region.

Irreversible inhibition of MIF by 2-OPB (7). The inactivation of the PPT activity of MIF by **7** appears to be a biphasic process where the inactivation occurs primarily within the first few seconds (data not shown). Moreover, the loss of activity is nearly stoichiometric (based on the subunit molecular mass of MIF). For example, at a $\sim 0.5:1$ ratio of inhibitor to protein, about 40% of the activity is lost within the first 5 s. At a $\sim 1:1$ ratio of inhibitor to protein, nearly 70% of the activity is lost within the first 5 s. At a $\sim 2:1$ ratio of inhibitor to protein, nearly 85% of the activity is lost within the first 5 s. Binding at the active site is suggested by the observation that **13** partially protects against inactivation. In the presence of a 250 μM solution of **13**, only $\sim 50\%$ of the PPT activity is lost in 120 s even though MIF was incubated with ~ 1.2 equiv. of **7**. Dialysis (68 h) does not result in significant reactivation of the PPT activity, consistent with the formation of a covalent bond between the enzyme and the adduct resulting from **7**.

Identification of the residue modified by 7. MIF was titrated with aliquots of **7** in order to determine the site of modification that results in the loss of PPT activity. After the addition of the third aliquot, corresponding to a ratio of $\sim 0.6:1$ inhibitor to protein, there was no detectable PPT activity.² The inactivated MIF and a control sample were purified by gel filtration chromatography and analyzed by ESI-MS. ESI-MS analysis of the untreated MIF showed a subunit molecular mass of 12,370.0 (± 6) Da, which is comparable to the expected subunit molecular mass of 12,373.1 Da (average mass). ESI-MS analysis of the inactivated MIF showed a subunit molecular mass of 12,544.0 Da. The difference between these masses (174.4 Da) indicates a single site of modification by one unit of a species with a mass of 174 ± 6 Da.

The site of the covalent modification was identified by subjecting MIF and the inactivated MIF to proteolytic digestion by trypsin and analyzing the resulting peptide mixtures by MALDI-TOF mass spectrometry (Fig. 1 and Table 2). The modified residue was determined by a comparative analysis of the spectra followed by selective fragmentation of the peptides of interest [27]. In both spectra, a peak is observed at m/z 1288.6, which corresponds to the calculated mass of the N-terminal sequence (PMFIVNTNVPR) (Fig. 1, Table 2). There is also a smaller peak at m/z 1304.6 attributed to the oxidation of Met-2 residue in the peptide. In the samples treated with **7**, there are additional peaks at m/z 1391.0, 1406.9, 1417.8, 1433.6, 1463.0, and 1479.3. The peaks appear in pairs spaced by 16 Da with the first peak being more intense than the second, suggesting that they are derived from a partially oxidized methionine-containing peptide. The peptide displaying a peak at m/z 1463.0 is 174.4 Da higher than the mass of the N-terminal sequence (PMFIVNTNVPR).³ The increase in mass is due to the covalent attachment of species with a mass of 174 Da.

² At a higher ratio of inhibitor to protein ($\sim 70:1$), 2 equiv. of inhibitor were covalently bound, as determined by ESI-MS analysis. ESI-MS analysis of the inactivated MIF showed subunit molecular masses of 12544.0 and 12718.0 Da. The differences between these masses and that of the unmodified MIF subunit are 174.0 and 348.0 Da, indicating modification of MIF by two molecules of **7**. The second site of modification was not identified.

³ Confirmatory results were obtained by subjecting MIF and MIF inactivated by **7** to digestion by endoproteinase Glu-C (protease V8), which cleaves at the carboxylate side of glutamate and aspartate residues (data not shown). In these experiments, the N-terminal peptide sequence is PMFIVNTNVPRASVPE with an average MW of 1772.1 Da.

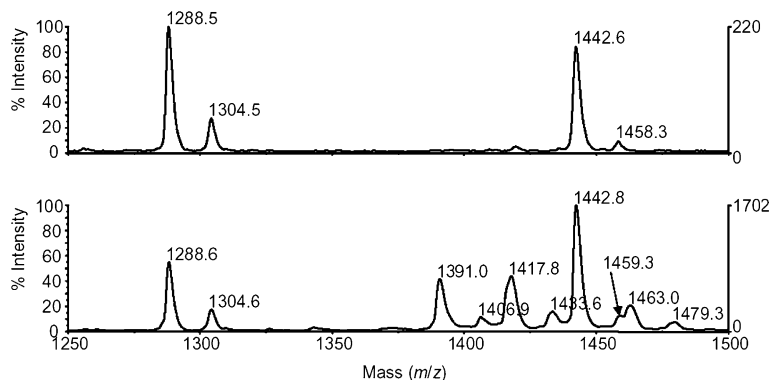


Fig. 1. MALDI MS spectra showing the region from m/z 1250–1500 for the tryptic digest of MIF (upper) and MIF treated with 7 (lower). In both panels, the peak at m/z 1288 corresponds to the N-terminal peptide “PMFIVNTNVPR”, and the peak at 1304 corresponds to the same sequence with an oxidized Met-2. The peaks at 1442 and 1458/1459 correspond to an unidentified protein that co-purified with MIF. The sample of MIF treated with 7 has additional peaks at 1391/1406 (+102 Da), 1417/1433 (a mix of +128/130 Da), and 1463/1479 (+174 Da). Assignments are presented in the text.

Table 2

Mass spectral analysis of the tryptic digest of MIF and MIF modified by 7^a

Obsd mass (Da) (control)	obsd mass (Da) (treated)	Peptide fragment	Mass difference (Da)
1288.9	1288.6	PMFIVNTNVPR	
1304.9	1304.6		16
	1391.0		102
	1406.9		11
	1417.8		129
	1433.6		145
1443.0	1442.8	Contaminant	
1458.9	1459.3		
	1463.0		174
	1479.3		190

^a Ions between 1200 and 1500 Da that are >5% of the base peak. Error is ± 0.5 Da.

The ions corresponding to the peaks at m/z 1288, 1391, and 1463 were subjected to MALDI-PSD fragmentation analysis to determine the amino acid sequence and location of the modified residue [27]. The MALDI-PSD spectra of the peak at m/z 1288 is consistent with its assignment to the N-terminal sequence of MIF, (PMFIVNTNVPR), by the matched b and y fragment ions (Fig. 2). The peptide at m/z 1391 was also subject to MALDI-PSD and matched to the same sequence, with the a and b ions shifted by 102 Da. The modified a2 and b3 ions, which retain charge on the N-terminal peptide fragments, indicate that modification occurs at or near the N-terminal of the peptide. A prominent ion at 172 can be assigned as the Pro-1 immonium ion with a modification of 102 Da. There is no fragment at 172 in the spectra of the unmodified peptides. The MALDI-PSD of the peptide at 1463 is dominated by neutral loss to 1390. The modification is observed only weakly as a 174 Da mass addition, but is more strongly observed as 102 and 128/130 mass addition peptides. These peptides likely form from the loss of COCOO from the inhibitor to form an adduct with a mass of 102 Da, and from the loss of HCOOH to form an adduct with a mass of 130 Da. The decomposition/rearrangement likely results from a

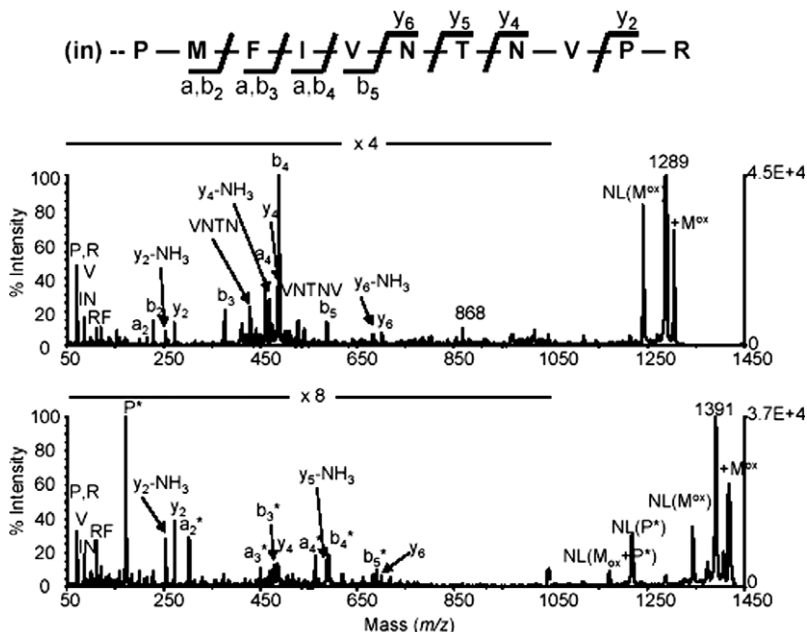


Fig. 2. MALDI-PSD spectra of the parent ions at m/z 1289 (upper) and 1391 (lower) from the tryptic digest of MIF treated with **7**. The spectra are matched to the N-terminal sequence, “PMFIVNTNVP” (where “in” designates the inhibitor). The upper panel shows the spectra for unmodified peptide whereas the lower panel shows the peptide modified by a mass addition of 102 Da. The modification is located on Pro-1, as determined by the presence of modified P immonium ion, and the a_2^* ions. In both spectra, the parent ion selection window captured Met-2 with and without the sulfoxide. The sulfoxide-modified peptide has an intense ion for neutral loss of CH_3SOH . In the lower panel, neutral loss of modified Pro-1 is also observed.

MALDI-MS related process. Similar decomposition of peptide-bound inhibitors has been observed previously [26].

The crystal structure of MIF soaked with 7. The overall structure of MIF determined in this study did not reveal any significant differences from previously reported MIF structures [13,14,31]. Superpositioning of this structure with that determined for the structure of mouse MIF in complex with the competitive inhibitor, *E*-2-fluoro-*p*-hydroxycinnamate (**13**) (PDB code 1MFI) [15] shows only 0.424 Å rmsd for 342 $\text{C}\alpha$ atoms and 0.47 Å rmsd for 1368 backbone atoms. Superpositioning of this structure with that determined for the human MIF structure (PDB code 1GD0) shows 0.326 Å rmsd for 342 $\text{C}\alpha$ atoms and 0.35 Å rmsd for 1368 backbone atoms [40].

The active site of MIF soaked with 7. Attempts to grow crystals of MIF that had been previously inactivated by **7** were not successful. Thus, crystals of native MIF were soaked in solutions of **7**, removed, and frozen before cracking. The trimer of MIF clearly shows three potential active site cavities, one near each Pro-1. Although excellent data were obtained (1.45 Å resolution, Fig. 3) and the MIF electron density was superb, the inhibitor density seen in two of the three active sites was ambiguous (Fig. 4). It is assumed that the inhibitor has decomposed under the crystallization conditions.

The third active site showed very distinct $2F_o - F_c$ density protruding into the active site cavity. The density corresponds to the side chain of Glu-16 from another trimer from

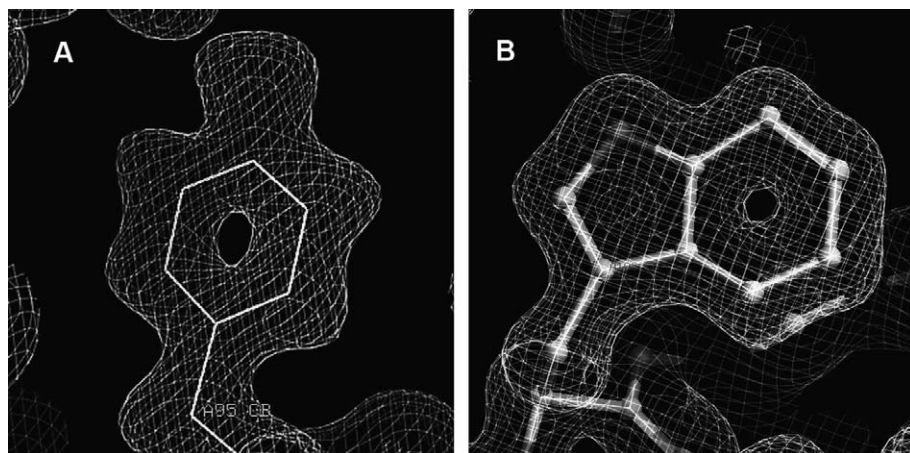


Fig. 3. Representative electron density showing the quality of data at 1.45 Å resolution. (A) The molecular replacement solution and the first electron density map were calculated using Y95F mutant coordinates (PDB code 1MFF, 2.0 Å resolution) for phases, whereas the protein contained the Tyr-95 residue, whose hydroxyl moiety was readily apparent. (B) Trp-108 after several cycles of unrestrained anisotropic refinement. The density shown for both views is $2F_o - F_c$ map contoured at 1.0σ . The figure was generated in graphics program O [37].

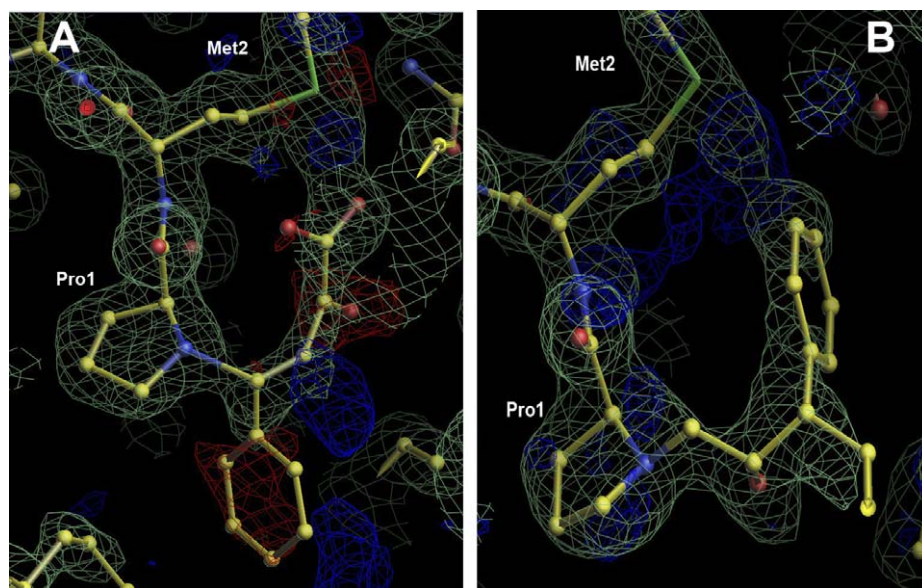


Fig. 4. Pro-1 adduct resulting from MIF crystals soaked with 7 modeled into the active site. (A) The expected Michael complex (i.e., 15, Scheme 4) between Pro-1 and 7 does not fit well into the observed electron density. (B) A Pro-1 adduct resulting from the MIF crystals soaked with 7 via a yet unidentified mechanism provides a much better fit. The green density is $2F_o - F_c$ map contoured at 1.0σ . The blue is $F_o - F_c$ positive density contoured at 2.5σ , and the red is negative density contoured at -2.8σ . The figure was generated by the program O [37].

a crystallographic symmetry mate in the $P6_3$ space group (Fig. 5A and B). The Glu-16 side chain appears to help stabilize four water molecules in the active site, but makes no direct contact with Pro-1. The distances between these four density centers (2.68, 2.77, 2.79, and

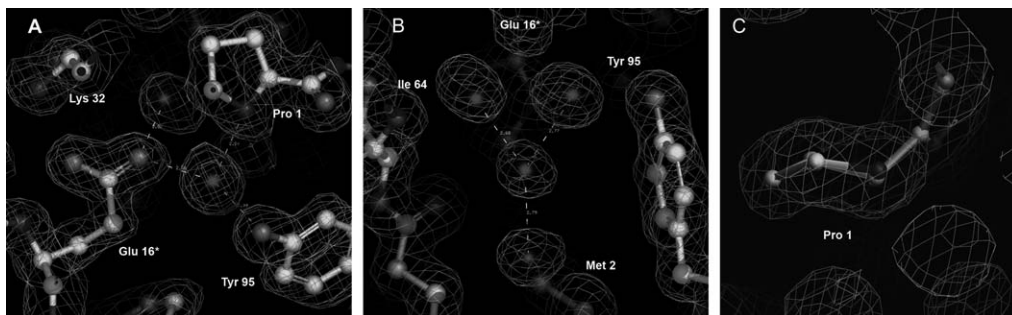


Fig. 5. Active site residues participating in crystal contact between trimers. (A) Glu-16' from a crystallographic symmetry mate protruding into the active site cavity. Two of the four bound solvent molecules are also visible. (B) A different view of the same site showing all four water molecules bound in the occluded active site. (C) A close-up of the occluded, inhibitor-free active site, showing the clearly defined proline pucker. The density for all three panels is $2F_o - F_c$ map contoured at 1.0σ . The figure was produced using the graphics program Pymol [41].

3.09 Å) correspond to hydrogen bond distances and not to carbon-carbon bonds. The two density centers closest to the catalytic proline are 3.13 and 2.80 Å from it, also suggesting hydrogen bonds involving waters and not a covalent adduct. Although this trimer-trimer contact may have contributed to the stability and high-resolution quality of these MIF crystals, the protruding Glu-16' side chain leaves little room for the inhibitor in that active site. Hence, attempts were made to crystallize the E16A mutant of MIF with and without **7**. Only crystals with no inhibitor could be grown, but at 30% PEG 8000. Unfortunately, these crystals cracked immediately upon the addition of **7**, suggesting that conformational changes involving crystal contacts take place upon the binding of **7**. The E16A-MIF crystallized in the same space group, $P6_3$, but these crystals did not diffract to sufficiently high-resolution to pursue a structure, suggesting that the trimer-trimer contact involving the side chain of Glu-16 is important for crystal quality and stability.

Nonetheless, the high-resolution of this active site clearly shows a pronounced pucker of the Pro-1 ring atoms (Fig. 5C), which have been implicated with the pK_a variation of Pro-1 [42]. This proline displays up (U) puckering, with C_γ atom in the exo position. The values for the torsion angles, as calculated by GEOMCALC [32] are $\chi^0 = 5.73^\circ$, $\chi^1 = -27.39^\circ$, $\chi^2 = 38.69^\circ$, $\chi^3 = -35.56^\circ$, $\chi^4 = 18.42^\circ$, $\varphi = -53.62^\circ$, as defined previously [43]. These values are in excellent agreement with previously determined dihedral angles of puckered prolyl residues [44]. The C_β atom shows virtually no puckering, as indicated by the small χ^0 angle, and is essentially in the plane defined by C_δ -N- C_α atoms.

4. Discussion

Analogues of 2-oxo acids (such as 2-ketoglutarate and pyruvate) are potential mechanistic probes of a wide variety of enzymes [45,46]. It is therefore not surprising that several such compounds have been synthesized and tested including the acetylene derivatives, 2-OP (**5**, Scheme 2), 2-OB (**6**), and 2-OPB (**7**) [18,19,45,46]. Chiu and Jordan first reported a synthesis for 2-OPB in which a lithium derivative of **8** was coupled with an oxalic ester [45]. However, we chose to adapt our procedure for the syntheses of 2-OP [18] and 2-OB [19] and generated **12**, in which the *t*-butyl group replaces the ethyl ester. The *t*-butyl ester can be removed under anhydrous conditions.

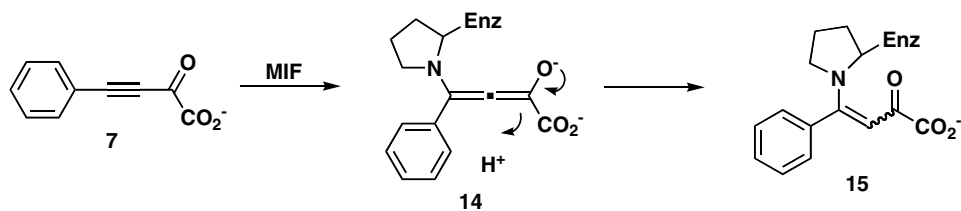
The subsequent incubation of **7** with MIF showed that the acetylene compound is a potent active-site-directed irreversible inhibitor of the PPT activity of MIF. Interestingly, a substoichiometric concentration of inhibitor (~ 0.5 equiv.) results in a complete loss of activity. Under these conditions, a single site on the protein is covalently modified. The site of modification is Pro-1, previously implicated as the catalytic base in the PPT activity of MIF [13,17].

One reasonable mechanism for the inactivation involves the Michael addition of the amino-terminal proline to the C-4 position of **7** (Scheme 4). Attack at this position produces an enol (or enolate, **14**), which tautomerizes to afford **15** [18]. The observation that the covalent adduct on Pro-1 has a molecular mass of 174 Da is consistent with the formation of **15**. Moreover, it is well known that α,β -unsaturated acetylenic ketones are susceptible to nucleophilic attack and the low pK_a for Pro-1 (~ 5.6) suggests that it can function as a nucleophile and react with **7** [18]. Modification of one of the three active sites in MIF apparently disrupts the remaining two active sites such that these sites no longer have PPT activity. The disruption of these active sites may result from conformational changes that occur as the bound linear acetylene molecule is transformed to a more flexible covalent adduct. It was anticipated that a crystallographic analysis might provide a structural rationale for these observations. However, the electron density observed in the two active sites that were not blocked by a neighboring Glu-16 does not appear to fit well when modeled with the expected Michael complex (Fig. 4A). Although it is believed that this might be due to the decomposition of inhibitor over time under the conditions used for crystallization, an unambiguous explanation for this density is lacking.

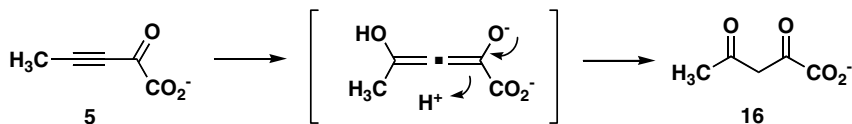
MIF is also categorized as a tautomerase superfamily member [16,47]. The tautomerase superfamily consists of five known families represented by MIF, 5-carboxymethyl-2-hydroxy-muconate isomerase (CHMI), 4-OT [16,47,48], *cis*-3-chloroacrylic acid dehalogenase (*cis*-CaaD) [49], and malonate semialdehyde decarboxylase (MSAD) [50]. CHMI, from *E. coli* C, and 4-OT, from *P. putida* mt-2, function as tautomerases in degradation pathways for aromatic amino acids and aromatic hydrocarbons, respectively [51]. *cis*-CaaD precedes MSAD in the degradation pathway for the nematocide, 1,3-dichloropropene [52].

A battery of mechanistic and structural studies has implicated Pro-1 as a critical catalytic residue in all characterized tautomerase superfamily members. Pro-1 can function as either a catalytic base {the PPT activity of MIF [13,15], CHMI [51], and 4-OT [53,54]} or an acid {CaaD [55], *cis*-CaaD [49,56], and MSAD [40,57]}, depending on the pK_a value, which is governed partly by the active site environment. The pK_a has been directly measured for 4-OT (~ 6.4) [54], MIF (~ 5.6) [58], CaaD [55] and MSAD (both ~ 9.2) [57] by ^{15}N NMR titration of the uniformly labeled enzyme.

In the absence of a direct NMR measurement of the pK_a value, 2-OP (**5**) has served as an effective indicator of the pK_a value and the active site environments of tautomerase



Scheme 4.



Scheme 5.

superfamily members. The reaction of 2-OP with superfamily members reflects the predominant ionization state of the catalytic proline (neutral vs. cationic) and the nature of the active site (hydrophobic vs hydrophilic). For example, 4-OT is inactivated by 2-OP (and 2-OB) [18,19], whereas CaaD, *cis*-CaaD, and MSAD process 2-OP to aceto-pyruvate (**16**, Scheme 5) although with different efficiencies [26,49,57]. In both enzymes, the addition of water to 2-OP results in the formation of an enol species. Subsequent keto-zation the enol produces **16**.

Likewise, 2-OPB could function as either an inhibitor or a substrate and may emerge as a useful mechanistic probe of tautomerase superfamily members. As an inhibitor, 2-OPB would inactivate MIF homologues with a PPT activity in which Pro-1 has a low pK_a value due to a hydrophobic active site. As a substrate, MIF homologues could add water to the C-4 position and generate benzoylpyruvate. Efforts are currently underway to identify tautomerase superfamily members capable of accommodating the larger phenyl ring and carrying out a conjugate addition of water.

Acknowledgments

The mass spectrometry described in this paper was carried out in the Analytical Instrumentation Facility Core housed in the College of Pharmacy at the University of Texas at Austin and supported by Center Grant ES07784.

References

- [1] M. George, J.H. Vaughan, Proc. Soc. Exp. Biol. Med. 111 (1962) 514–521.
- [2] B.R. Bloom, B. Bennett, Science 153 (1966) 80–82.
- [3] J.R. David, Proc. Natl. Acad. Sci. USA 56 (1966) 72–77.
- [4] M. Leech, C. Metz, L. Santos, T. Peng, S.R. Holdsworth, R. Bucala, E.F. Morand, Arthritis Rheum. 41 (1998) 910–917.
- [5] M. Leech, C. Metz, P. Hall, P. Hutchinson, K. Gianis, M. Smith, H. Weedon, S.R. Holdsworth, R. Bucala, E.F. Morand, Arthritis Rheum. 42 (1999) 1601–1608.
- [6] T. Mikayama, T. Nakano, H. Gomi, Y. Nakagawa, Y.C. Liu, M. Sato, A. Iwamatsu, Y. Ishii, W.Y. Weiser, K. Ishizaka, Proc. Natl. Acad. Sci. USA 90 (1993) 10056–10060.
- [7] S. Onodera, K. Kaneda, Y. Mizue, Y. Koyama, M. Fujinaga, J. Nishihira, J. Biol. Chem. 275 (2000) 444–450.
- [8] H.Y. Lan, W. Mu, N. Yang, A. Meinhardt, D.J. Nikolic-Paterson, Y.Y. Ng, M. Bacher, R.C. Atkins, R. Bucala, Am. J. Pathol. 149 (1996) 1119–1127.
- [9] J. Bernhagen, T. Calandra, R.A. Mitchell, S.B. Martin, K.J. Tracey, W. Voelter, K.R. Manogue, A. Cerami, R. Bucala, Nature 365 (1993) 756–759.
- [10] M. Bozza, A.R. Satoskar, G. Lin, B. Lu, A.A. Humbles, C. Gerard, J.R. David, J. Exp. Med. 189 (1999) 341–346.
- [11] T. Calandra, J. Bernhagen, R.A. Mitchell, R. Bucala, J. Exp. Med. 179 (1994) 1895–1902.
- [12] E. Rosengren, P. Aman, S. Thelin, C. Hansson, S. Ahlfors, P. Bjork, L. Jacobsson, H. Rorsman, FEBS Lett. 417 (1997) 85–88.

- [13] J.B. Lubetsky, M. Swope, C. Dealwis, P. Blake, E. Lolis, *Biochemistry* 38 (1999) 7346–7354.
- [14] M. Suzuki, H. Sugimoto, A. Nakagawa, I. Tanaka, J. Nishihira, M. Sakai, *Nat. Struct. Biol.* 3 (1996) 259–266.
- [15] A.B. Taylor, W.H. Johnson Jr., R.M. Czerwinski, H.S. Li, M.L. Hackert, C.P. Whitman, *Biochemistry* 38 (1999) 7444–7452.
- [16] C.P. Whitman, *Arch. Biochem. Biophys.* 402 (2002) 1–13.
- [17] S.L. Stamps, M.C. Fitzgerald, C.P. Whitman, *Biochemistry* 37 (1998) 10195–10202.
- [18] W.H. Johnson Jr., R.M. Czerwinski, M.C. Fitzgerald, C.P. Whitman, *Biochemistry* 36 (1997) 15724–15732.
- [19] A.B. Taylor, R.M. Czerwinski, W.H. Johnson Jr., C.P. Whitman, M.L. Hackert, *Biochemistry* 37 (1998) 14692–14700.
- [20] M.C. Pirrung, J. Chen, E.G. Rowley, A.T. McPhail, *J. Am. Chem. Soc.* 115 (1993) 7103–7110.
- [21] S.C. Wang, W.H. Johnson Jr., R.M. Czerwinski, C.P. Whitman, *Biochemistry* 43 (2004) 748–758.
- [22] J. Sambrook, E.F. Fritsch, T. Maniatis, *Molecular Cloning: A Laboratory Manual*, Cold Spring Harbor Laboratory, Cold Spring Harbor, New York, 1989.
- [23] U.K. Laemmli, *Nature* 227 (1970) 680–685.
- [24] W.J. Waddell, *J. Lab. Clin. Med.* 48 (1956) 311–314.
- [25] S.N. Ho, H.D. Hunt, R.M. Horton, J.K. Pullen, L.R. Pease, *Gene* 77 (1989) 51–59.
- [26] S.C. Wang, M.D. Person, W.H. Johnson Jr., C.P. Whitman, *Biochemistry* 42 (2003) 8762–8773.
- [27] M.D. Person, T.J. Monks, S.S. Lau, *Chem. Res. Toxicol.* 16 (2003) 598–608.
- [28] Z. Otwinowski, W. Minor, in: C.W. Carter Jr., R.M. Sweet (Eds.), *Methods in Enzymology*, vol. 276, Academic Press, New York, 1997, pp. 307–326.
- [29] B.W. Matthews, *J. Mol. Biol.* 33 (1968) 491–497.
- [30] K.A. Kantardjiev, B. Rupp, *Protein Sci.* 12 (2003) 1865–1871.
- [31] S.L. Stamps, A.B. Taylor, S.C. Wang, M.L. Hackert, C.P. Whitman, *Biochemistry* 39 (2000) 9671–9678.
- [32] Collaborative Computational Project, Number 4, *Acta Crystallogr. D* 50 (1994) 760–763.
- [33] E. Potterton, P. Briggs, M. Turkenburg, E. Dodson, *Acta Crystallogr. D* 59 (2003) 1131–1137.
- [34] J. Navaza, *Acta Crystallogr. A* 50 (1994) 157–163.
- [35] G.N. Murshudov, A.A. Vagin, E.J. Dodson, *Acta Crystallogr. D* 53 (1997) 240–255.
- [36] M.D. Winn, M.N. Isupov, G.N. Murshudov, *Acta Crystallogr. D* 57 (2001) 122–133.
- [37] T.A. Jones, J.Y. Zou, S.W. Cowan, M. Kjeldgaard, *Acta Crystallogr. A* 47 (1991) 110–119.
- [38] R.J. Read, A.J. Schierbeek, *J. Appl. Crystallogr.* 21 (1988) 490–495.
- [39] A. Perrakis, R. Morris, V.S. Lamzin, *Nat. Struct. Biol.* 6 (1999) 458–463.
- [40] N. Guex, M.C. Peitsch, *Electrophoresis* 18 (1997) 2714–2723.
- [41] W.L. DeLano, *The Pymol Molecular Graphics System*, DeLano Scientific, San Carlos, CA, USA, 2002.
- [42] N. Panasiak Jr., E.S. Eberhardt, A.S. Edison, D.R. Powell, R.T. Raines, *Int. J. Pept. Protein Res.* 44 (1994) 262–269.
- [43] F.A. Momany, R.F. McGuire, A.W. Burgess, H.A. Scheraga, *J. Phys. Chem.* 79 (1975) 2361–2381.
- [44] G. Nemethy, K.D. Gibson, K.A. Palmer, C.N. Yoon, G. Paterlini, A. Zagari, S. Rumsey, H.A. Scheraga, *J. Phys. Chem.* 96 (1992) 6472–6484.
- [45] C.C. Chiu, F. Jordan, *J. Org. Chem.* 59 (1994) 5763–5766.
- [46] A. Brown, N. Nemeria, J. Yi, D. Zhang, W.B. Jordan, R.S. Machado, J.R. Guest, F. Jordan, *Biochemistry* 36 (1997) 8071–8081.
- [47] A.G. Murzin, *Curr. Opin. Struct. Biol.* 6 (1996) 386–394.
- [48] J.J. Almrud, A.D. Kern, S.C. Wang, R.M. Czerwinski, W.H. Johnson Jr., A.G. Murzin, M.L. Hackert, C.P. Whitman, *Biochemistry* 41 (2002) 12010–12024.
- [49] G.J. Poelarends, H. Serrano, M.D. Person, W.H. Johnson Jr., A.G. Murzin, C.P. Whitman, *Biochemistry* 43 (2004) 759–772.
- [50] G.J. Poelarends, W.H. Johnson Jr., A.G. Murzin, C.P. Whitman, *J. Biol. Chem.* 278 (2003) 48674–48683.
- [51] H.S. Subramanya, D.I. Roper, Z. Dauter, E.J. Dodson, G.J. Davies, K.S. Wilson, D.B. Wigley, *Biochemistry* 35 (1996) 792–802.
- [52] G.J. Poelarends, M. Wilkens, M.J. Larkin, J.D. van Elsas, D.B. Janssen, *Appl. Environ. Microbiol.* 64 (1998) 2931–2936.
- [53] J.T. Stivers, C. Abeygunawardana, A.S. Mildvan, G. Hajipour, C.P. Whitman, L.H. Chen, *Biochemistry* 35 (1996) 803–813.
- [54] J.T. Stivers, C. Abeygunawardana, A.S. Mildvan, G. Hajipour, C.P. Whitman, *Biochemistry* 35 (1996) 814–823.

- [55] H.F. Azurmendi, S.C. Wang, M.A. Massiah, G.J. Poelarends, C.P. Whitman, A.S. Mildvan, *Biochemistry* 43 (2004) 4082–4091.
- [56] G.J. Poelarends, H. Serrano, W.H. Johnson Jr., C.P. Whitman, *Biochemistry* 43 (2004) 7187–7196.
- [57] G.J. Poelarends, H. Serrano, W.H. Johnson Jr., D.W. Hoffman, C.P. Whitman, *J. Am. Chem. Soc.* 126 (2004) 15658–15659.
- [58] M. Swope, H.W. Sun, P.R. Blake, E. Lolis, *EMBO J.* 17 (1998) 3534–3541.